

# Selection Effects on the Observed Redshift Dependence of GRB Jet Opening Angles

Rui-Jing Lu<sup>1</sup>, Jun-Jie Wei<sup>1</sup>, Shu-Fu Qin<sup>2</sup> and En-Wei Liang<sup>\*1,2</sup>

## ABSTRACT

Apparent redshift dependence of the jet opening angles ( $\theta_j$ ) of gamma-ray bursts (GRBs) is observed from current GRB sample. We investigate whether this dependence can be explained with instrumental selection effects and observational biases by a bootstrapping method. Assuming that (1) the GRB rate follows the star formation history and the cosmic metallicity history and (2) the intrinsic distributions of the jet-corrected luminosity ( $L_\gamma$ ) and  $\theta_j$  are a Gaussian or a power-law function, we generate a mock *Swift*/BAT sample by considering various instrumental selection effects, including the flux threshold and the trigger probability of BAT, the probabilities of a GRB jet pointing to the instrument solid angle and the probability of redshift measurement. Our results well reproduce the observed  $\theta_j - z$  dependence. We find that in case of  $L_\gamma \propto \theta_j^2$  good consistency between the mock and observed samples can be obtained, indicating that both  $L_\gamma$  and  $\theta_j$  are degenerate for a flux-limited sample. The parameter set  $(L_\gamma, \theta_j) = (4.9 \times 10^{49} \text{erg s}^{-1}, 0.054 \text{rad})$  gives the best consistency for the current *Swift* GRB sample. Considering the beaming effect, the derived intrinsic local GRB rate accordingly is  $2.85 \times 10^2 \text{Gpc}^{-3} \text{yr}^{-1}$ , inferring that  $\sim 0.59\%$  of Type Ib/c SNe may be accompanied by a GRB.

*Subject headings:* Gamma-ray burst: general—Methods: statistical—Stars: formation

## 1. Introduction

Gamma-ray bursts (GRBs) are the most luminous explosions in the Universe. They are detected from deep to our local Universe (Zhang & Meszaros 2004). The measured redshifts

---

<sup>1</sup>Department of Physics and GXU-NAOC Center for Astrophysics and Space Sciences, Guangxi University, Nanning 530004, China; lew@gxu.edu.cn

<sup>2</sup>The National Astronomical Observatories, Chinese Academy of Sciences, Beijing 100012, China

of current GRB sample range from 0.0085 (GRB 980425; Tinney et al. 1998) to 8.2 (GRB 090423; Tanvir et al. 2009)<sup>1</sup>. It is generally believed that the births of long GRBs follow the star formation history of the universe (e.g., Totani 1997; Paczynski 1998; Bromm & Loeb 2002; Lin et al. 2004), and they may be promising probes for cosmology and galaxy evolution (e.g., Dai et al. 2004; Ghirlanda et al. 2004; Liang et al. 2005; Yüksel & Kistler 2007; Kistler et al. 2008, 2009; Salvaterra et al. 2008; Wang & Dai 2009). However, it is still unclear if GRBs experience any sort of cosmic evolution.

With high sensitivity of the burst alert telescope (BAT) and the promptly slewing capability of the narrow-field X-ray telescope (XRT) onboard the *Swift* satellite (Gehrels et al. 2004), the number of measured high- $z$  GRBs has increased rapidly over the last 6.5 years. It is found that long GRBs do not follow star formation rate (SFR) unbiasedly (e.g., Kistler et al. 2008). The observed GRB rate is higher than the SFR at  $z \sim 4$ , which may be due to that the GRB rate is also related to the cosmic metallicity history (Kistler et al. 2008; Li 2008; Qin et al. 2010; Virgili et al. 2011) or due to a higher efficiency of long GRB production rate by massive stars at high- $z$  (Daigne et al. 2006). It was also suggested that the GRB luminosity may evolve with redshift, being more luminous in the past, which is simplified as  $L \propto L_0(1+z)^\delta$ , where  $L_0$  is the luminosity of local GRBs (Lloyd-Ronning, Fryer & Ramirez-Ruiz 2002; Firmani et al. 2004; Kocevski & Liang 2006; Salvaterra et al. 2008, 2009).

It is believed that GRBs should be collimated into narrow jets (Rhoads 1997). The collimation of GRB jet is critical to understand the physics of GRBs, such as their central engine, intrinsic GRB rate, and true gamma-ray energy explosion (e.g., Zhang et al. 2004). The observed steepening with a decay slope of  $\sim 2$  in the late afterglow lightcurves is possibly due to the jet effect, in which a break would happen when the bulk Lorentz factor of the outflow ( $\Gamma$ ) slows down to  $\Gamma < \theta_j^{-1}$ , where  $\theta_j$  is the half opening angle of the jet (Rhoads 1997; Sari et al. 1999). With the observed jet break time  $t_j$ , the  $\theta_j$  can be calculated (Rhoads 1997; Chevalier & Li 2000). Frail et al. (2001) derived the geometrically-corrected gamma-ray energy ( $E_\gamma$ ) of a small GRB sample and proposed an idea of a standard energy reservoir in GRB jets based on the narrow distribution of  $E_\gamma$  (see also Berger et al. 2003 for the same conclusion for the jet-corrected luminosity ( $L_\gamma$ )). However, this result seems to be a sample selection effect. The  $E_\gamma$  distribution is significantly broadened with the current GRB sample, although it is still log-normal (Liang et al. 2008; Racusin et al. 2010). It was also proposed that GRB jet opening angles may experience similar kind of evolution as GRB luminosity (Wei et al. 2003). Estimated the  $\theta_j$  of the BATSE GRB sample with an empirical

---

<sup>1</sup>A photometric redshift of 9.4 for GRB 090429B was reported by Cucchiara et al. (2011)

relation based on the Yonetoku and Ghirlanda relations (Ghirlanda et al. 2004; Yonetoku et al. 2004), Yonetoku et al. (2005) argued that  $\theta_j$  evolves as  $\theta_j \propto (1+z)^{-0.45}$ .

The evolution features of GRB luminosity and jet opening angle as well as the GRB jet energy distribution are based on the statistics for the current observational samples. However, as well known, observational samples highly suffers instrumental selection effects and observations biases (Bloom 2003). It is difficult to reveal the intrinsic distributions and evolution features of GRBs from these samples. For example, a GRB with a peak photon flux lower than an instrumental threshold cannot trigger the instrument. Even the flux is over the threshold, the trigger probability of a GRB strongly depends on its photon flux (Qin et al. 2010). The probability of a GRB jet pointing to the solid angle of an instrument is different for GRBs with different  $\theta_j$ . In addition,  $E_\gamma$  (or  $L_\gamma$ ) and  $\theta_j$  are not direct observable. The derivations of these parameters are mainly based on the observed flux, redshift, and  $t_j$ . However, both  $E_\gamma$  (or  $L_\gamma$ ) and  $\theta_j$  are degenerate for a flux-limited sample. This means that an intrinsically dimmer GRB (with lower  $E_\gamma$  or  $L_\gamma$ ) may be detected by a given instrument in case of a smaller  $\theta_j$ .

In this paper we investigate whether the observed redshift dependences of jet opening angles and isotropic gamma-ray luminosity of long GRBs can be explained with instrumental selection effects and observational biases. Based on our results we also estimate the local long GRB rate by considering the beaming effect. We search for GRBs whose jet break times in afterglow lightcurves are reported in literature. The data are reported in Section 2. Our models and results for *Swift*/BAT sample are reported in section 3. Conclusions and Discussion are presented in Section 4. Throughout we use cosmological parameters  $H_0 = 71 \text{ km s}^{-1} \text{ Mpc}^{-1}$ ,  $\Omega_M = 0.3$ ,  $\Omega_\Lambda = 0.7$ .

## 2. Data

Our sample includes all GRBs whose jet break times ( $t_j$ ) are measured in the radio, optical, and X-ray afterglow lightcurves, regardless the  $t_j$  are achromatic, or just detected only in one band. Note that a tentative achromatic jet breaks in the radio, optical and X-ray afterglow lightcurves are available for three GRBs. We take the  $t_j$  of these GRBs measured in the optical afterglow lightcurves. Seventy-seven GRBs are included in our sample. They are summarized in Table 1. Since different cosmological parameters and medium density surrounding the bursts are used in calculations of  $\theta_j$  in literature, we re-derive  $E_{\text{iso}}$ ,  $\theta_j$ , and  $E_\gamma$  in a consistent method with the same cosmological parameters and the same jet model

for a constant medium density (Rhoads 1997, Sari et al. 1999, Frail et al. 2001)

$$\theta_j = 0.057 \text{rad} \left( \frac{t_j}{1 \text{ day}} \right)^{3/8} \left( \frac{1+z}{2} \right)^{-3/8} \left( \frac{E_{\text{iso}}}{10^{53} \text{ ergs}} \right)^{-1/8} \left( \frac{\eta_\gamma}{0.2} \right)^{1/8} \left( \frac{n}{0.1 \text{ cm}^{-3}} \right)^{1/8}, \quad (1)$$

where  $n$  is the ambient medium density in unit of  $\text{cm}^{-3}$  and  $\eta_\gamma$  is the efficiency of the fireball in converting the energy in the ejecta into gamma-rays. We take  $\eta_\gamma = 0.2$  and  $n \sim 0.1 \text{ cm}^{-3}$  in our calculations. The  $E_{\text{iso}}$  is calculated with

$$E_{\text{iso}} = \frac{4\pi D_L^2 S_\gamma}{(1+z)} k, \quad (2)$$

where  $S_\gamma$  is the observed gamma-ray fluence,  $D_L$  is the luminosity distance at redshift  $z$ , and  $k$  is a factor to correct the observed gamma-ray energy in a given band pass to a broad band (i.e.,  $1 - 10^4$  keV in this analysis) with the observed GRB spectra (Bloom et al. 2001). We collect the spectral parameters for the burst in our sample from literature. It is well known that the GRB spectrum is well fit with the Band function (Band et al. 1993). Since the narrowness of the *Swift*/BAT band, the spectra of most *Swift* GRBs in our sample are adequately fit with a single power-law,  $N \propto E^{-\Gamma}$  (Zhang et al. 2007; Sakamoto et al. 2009). If the parameters of the Band function are unavailable for the *Swift* GRBs, we use an empirical relation between the peak energy of the  $\nu f_\nu$  spectrum and the photon index  $\Gamma$ , i.e.  $\log E_p = (2.76 \pm 0.07) - (3.61 \pm 0.26) \log \Gamma$  (Zhang et al. 2007), to estimate the  $E_p$  and take the low and high photon indices as  $\alpha = -1.1$  and  $\beta = -2.2$  (Preece et al. 2000; Kaneko et al. 2006). The geometrically-corrected gamma-ray energy of a GRB jet can be obtained with

$$E_\gamma = (1 - \cos \theta_j) E_{\text{iso}}. \quad (3)$$

The derived  $\theta_j$  and  $E_\gamma$  are reported in Table 1. It is found that their distributions are log-normal, as shown in Figure 1. The fits with a Gaussian function yield  $\log(\theta_j/\text{rad}) = (-1.31 \pm 0.24) (1\sigma)$  and  $\log(E_\gamma/\text{erg}) = (50.07 \pm 0.91) (1\sigma)$ , respectively. The  $\theta_j$  as a function of  $z$  is shown in Figure 2. A tentative anti-correlation is observed. The best fit gives

$$\log \theta_j = (-0.90 \pm 0.09) - (0.94 \pm 0.19) \log(1+z), \quad (4)$$

with a Spearman correlation coefficient of 0.55, a standard deviation of 0.30, and a chance probability  $p < 10^{-4}$  for  $N = 77$ .

### 3. Analysis of the Instrumental Selection Effects

It is unclear whether the observed  $\theta_j - z$  dependence shown above is due to observational selection effects or due to an intrinsic cosmological evolution feature of GRBs. In this section, we make bootstrap analysis of the instrumental selection effects on this dependence.

### 3.1. Models

The number density of GRBs at redshift  $z \sim z + dz$  is given by

$$n(z, L_\gamma) = \frac{dN}{dz dL_\gamma dT} = \frac{R_{\text{GRB}}(z) dV(z)}{1+z} \frac{dV(z)}{dz} \Phi(L_\gamma), \quad (5)$$

where  $R_{\text{GRB}}(z)$  is the co-moving GRB rate as a function of  $z$ , the factor  $(1+z)^{-1}$  accounts for the cosmological time dilation of the observed rate,  $dT$  is the time interval,  $\Phi(L_\gamma)$  is the luminosity function of GRB jets and  $dV(z)/dz$  is the co-moving volume element. We assume  $R_{\text{GRB}}$  traces the star formation rate and metallicity history, reading as (Kistler et al. 2008; Li 2008; Qin et al. 2010; Virgili et al. 2011)

$$R_{\text{GRB}}(z) = \rho_0 R_{\text{SFR}}(z) \Theta(\epsilon, z), \quad (6)$$

where  $\rho_0$  is the local GRB rate,  $\Theta(\epsilon, z)$  is the fractional mass density belonging to metallicity below  $\epsilon Z_\odot$  at a given  $z$  ( $Z_\odot$  is the solar metal abundance) and  $\epsilon$  is determined by the metallicity threshold for the production of GRBs. In our analysis, the  $R_{\text{SFR}}(z)$  is taken as

$$R_{\text{SFR}}(z) \propto \begin{cases} (1+z)^{3.44}, & z \leq z_{\text{peak}} \\ (1+z_{\text{peak}})^{3.44}, & z > z_{\text{peak}} \end{cases}, \quad (7)$$

where  $z_{\text{peak}} = 1$  (Rowan-Robinson 1999). The  $\Theta(\epsilon, z)$  is parameterized as (Hopkins & Beacom 2006; Langer & Norman 2006)

$$\Theta(\epsilon, z) = \frac{\hat{\Gamma}(\alpha + 2, \epsilon^\beta 10^{0.15\beta z})}{\Gamma(\alpha + 2)}, \quad (8)$$

where  $\alpha$  and  $\beta$  are the low and high spectral indices of the prompt gamma-rays,  $\hat{\Gamma}(a, x)$  and  $\Gamma(x)$  are the incomplete and complete gamma function (Langer & Norman 2006; Kistler et al. 2008). We adopt the jet-corrected luminosity function  $\Phi(L_\gamma)$  as a log-normal distribution function (Matsubayashi et al. 2005),

$$\Phi(L_\gamma) = \frac{A_L}{\sqrt{2\pi}\sigma_{L_\gamma}} \exp\left[-\frac{(\log L_\gamma - \log L_c)^2}{2\sigma_{L_\gamma}^2}\right], \quad (9)$$

where  $A_L$  is a normalized constant,  $L_c$  is the center value and  $\sigma_{L_\gamma}$  is the width of the distribution. The intrinsic distribution of  $\theta_j$  is unknown. We also take it as a log-normal distribution <sup>2</sup>,

$$\psi(\theta_j) = \frac{A_\theta}{\sqrt{2\pi}\sigma_\theta} \exp\left[-\frac{(\log \theta_j - \log \theta_c)^2}{2\sigma_\theta^2}\right], \quad (10)$$

---

<sup>2</sup>The case of a broken power-law and a power-law distributions for  $L_\gamma$  and  $\theta_j$ , respectively, is discussed in section 4.

where  $A_\theta$  is a normalized constant,  $\theta_c$  is the center value and  $\sigma_\theta$  is the width of the distribution. The observed peak flux in a given instrumental band for a GRB that has a half-opening angle  $\theta_j$  and jet-corrected luminosity  $L_\gamma$  at redshift  $z$  is derived from

$$P(z, L_\gamma, \theta_j) = \frac{L}{4\pi D_L^2(z)k} = \frac{L_\gamma}{4\pi D_L^2(z)(1 - \cos \theta_j)k}, \quad (11)$$

where  $L = L_\gamma/(1 - \cos \theta_j)$ .

The algorithm of the Swift/BAT trigger has two modes, the count rate trigger and image trigger (Fenimore et al. 2003; Sakamoto et al. 2008, 2011). Rate triggers are measured on different time scales (4 msec - 64 sec), with a single or several backgrounds. Image triggers are found by summing images over various timescales and searching for un-catalogued sources. Band (2006) compared the threshold of Swift/BAT in count rate mode with other GRB missions. The image trigger depends on the duration of a burst. Sakamoto et al. (2008) parameterized the threshold of BAT as a function of burst duration. With the triggered and off-line scanned samples of CGRO/BATSE, Qin et al. (2010) simplified the trigger probability as a function of the observed peak flux for BATSE. They took the same trigger probability for BAT to make bootstrap analysis for the BAT sample. In this analysis, we take a modified form of the trigger probability as proposed by Qin et al. (2010). As shown by Sakamoto et al. (2008), the trigger probability of the image trigger mode for those long GRBs with a low peak photon flux would be increased. In order to increase the trigger probability of long and weak GRBs that have a peak flux near the BAT threshold with the image trigger mode, we take the BAT trigger probability as a function of  $P$  as following<sup>3</sup>,

$$\eta_t(P) = \begin{cases} P^2 & P < 0.45 \quad \text{ph/cm}^2/\text{s} \\ 0.67(1.0 - 0.40/P)^{0.52}, & P \geq 0.45 \quad \text{ph/cm}^2/\text{s} \end{cases}. \quad (12)$$

The probability of redshift measurement for a GRB is complicated and depends on many parameters (Fynbo et al. 2009). It is difficult to parameterize the redshift measurement. Qin et al. (2010) got a weak dependence of the probability on the observed peak flux, which is quoted as following,

$$\eta_z(P) = 0.26 + 0.032e^{1.61 \log P}. \quad (13)$$

The probability of the alignment for a GRB with jet opening angle  $\theta_j$  to an instrument with a solid angle  $\Omega$  for the aperture flux is estimated with

$$\eta_a(\theta_j) = \frac{\Omega}{4\pi}(1 - \cos \theta_j). \quad (14)$$

---

<sup>3</sup>Note that we focus on the redshift-known sample in this analysis. These GRBs are usually bright. Therefore, some uncertainties of the trigger probability of weak GRBs near the instrumental threshold would be not significantly affected our analysis results.

Therefore, the number of GRBs with redshift measurement that trigger an instrument in an operation period  $T$  can be calculated with

$$N = T \int_0^{\pi/2} \psi(\theta_j) d\theta_j \int_{L_{\gamma, \min}}^{L_{\gamma, \max}} \eta_t(P) \eta_z(P) \eta_a(\theta_j) \Phi(L_{\gamma}) dL_{\gamma} \times \int_0^{z_{\max}} \frac{R_{GRB}(z)}{1+z} \frac{dV(z)}{dz} dz, \quad (15)$$

where  $z_{\max}$  is determined by the instrumental threshold of the peak flux ( $P_{\text{th}}$ ) for a given burst with luminosity  $L_{\gamma}$  according to equation (11). The  $L_{\gamma, \min}$  and  $L_{\gamma, \max}$  in our analysis are taken as  $10^{46}$  and  $10^{52}$  erg s $^{-1}$ , respectively.

### 3.2. Reference Sample for Constraining Model Parameters

Free parameters in our models are  $\rho_0$ ,  $L_c$  (and its deviation  $\sigma_{L_{\gamma}}$ ),  $\theta_c$  (and its deviation  $\sigma_{\theta}$ ) and  $\epsilon$ . We take the current *Swift*/BAT GRB sample as a reference sample to constrain these parameters. *Swift*/BAT has detected 670 GRBs by June 2011. Among them 170 GRBs have redshift measurement. We bootstrap a mock *Swift* GRB sample and compare it with the observations. The peak fluxes, redshift and the spectral information for these GRBs are taken from published BAT catalogs (Sakamoto et al. 2008; Sakamoto et al. 2009; Sakamoto et al. 2011). The peak fluxes are measured in 1-s timescale. Note that the low-luminosity GRBs ( $L < 10^{49}$  erg s $^{-1}$ ) are not included since they may belong to a distinct population (Soderberg et al. 2004; Liang et al. 2007; Chapman et al. 2007).

### 3.3. Bootstrapping Procedure

(1) Generate a mock GRB characterized by  $z$ ,  $L_{\gamma}$ , and  $\theta_j$ . These parameters are randomly from the probability distributions of Eqs. (6), (9), and (10) for a given set of model parameters ( $L_c$ ,  $\sigma_{L_{\gamma}}$ ,  $\theta_c$ ,  $\sigma_{\theta}$ ,  $\epsilon$ ). Since  $z < 10$  for the current BAT sample, the range of  $z$  for our analysis is from 0 to 10.

(2) Calculate the isotropic gamma-ray luminosity with  $L = L_{\gamma}/(1 - \cos\theta_j)$  and derive  $E'_p$  in the burst frame with an  $L - E'_p$  relation, i.e.  $E'_p = 200 \text{ keV}(L/10^{52})^{1/2}/C$ , where  $C$  is randomly distributed in [0.1, 1] (Liang et al. 2004).

(3) Calculate the peak flux in the *Swift*/BAT band with Eq. 11 assuming that the photon indices in the energy bands lower and higher  $E_p$  are -1 and -2.25, respectively (Preece et al. 2000), and compare it with the threshold of *Swift*/BAT. A mock GRB is recognized as detectable if its peak flux is over the threshold.

(4) Calculate the detection probability of a detectable GRB with the probabilities described by Equations (12), (13) and (14).

(5) Repeat the above steps to make a mock redshift-known BAT GRB sample (170 GRBs).

(6) Evaluate the consistency between the mock and the observed sample by comparing the  $z$ ,  $L$ , and  $\log N - \log P$  distributions. We measure the consistency with the K-S test. We calculate the probabilities of the K-S tests,  $P_{K-S}^P$ ,  $P_{K-S}^L$  and  $P_{K-S}^z$ , for the  $\log N - \log P$ ,  $L$  and  $z$  distributions and then define the global  $K - S$  test probability as  $P_{K-S}^G = P_{K-S}^P \times P_{K-S}^z \times P_{K-S}^L$ . A larger value of  $P_{K-S}$  indicates a better consistency. A value of  $P_{K-S} > 0.1$  is generally acceptable to claim the statistical consistency, whereas a value of  $P_{K-S} < 10^{-4}$  convincingly rejects the hypothesis of the consistency.

### 3.4. Results

Following the procedure described above we search for the model parameters that can present the best consistency between the mock and the observed BAT GRB samples. In order to reduce the amount of calculation, we first randomly generate a large sample of the parameter sets ( $L_c, \sigma_{L_\gamma}, \theta_c, \sigma_\theta, \epsilon$ ) in wide parameter ranges. Please note that we do not need to consider  $\rho_0$  in our bootstrap analysis since we make the comparisons between our results and observations with the relative probability distributions. We find that  $(\sigma_{L_\gamma}, \sigma_\theta, \epsilon) = (0.4, 0.6, 0.4)$  can well reproduce the scattering of the GRB distributions in the  $L - (1 + z)$  plane. We therefore fix the three parameters and then refine our search for the parameters  $L_c$  and  $\theta_c$ . Figure (3a) shows the contours of the relative  $P_{K-S}^G$  in the  $\log L_c - \log \theta_c$  plane. From Figure (3a) one can find that both  $\theta_c$  and  $L_c$  seem to be degenerate. If  $\theta_c \propto L_c^{0.5}$ , our results roughly reproduce the observations. This is reasonable based on the equation (11). It shows that for a given instrumental threshold  $P_{th}$ , a lower- $L_\gamma$  GRB may be detectable if its  $\theta_j$  is smaller. Therefore, one cannot constrain the intrinsic  $L_c$  and  $\theta_c$  based on a flux-limit sample. The parameter set  $(\log L_c/\text{erg s}^{-1}, \log \theta_c/\text{rad}) = (49.69, -1.27)$  gives the best consistency to the current *Swift*/BAT sample. Figure 4 displays the comparisons between our mock sample with the BAT sample in the  $\log L - \log(1 + z)$  plane along with the distributions of  $\log N - \log P$ ,  $L$ , and  $z$ . The  $P_{K-S}$  values for the  $\log L$ ,  $\log(1 + z)$  and  $\log N - \log P$  distributions are also marked in each panel. One can observe that the observed BAT sample can be well reproduced with our bootstrapping method. In order to get a robust results, we also generate a large sample of  $10^4$  GRBs with the best parameter set and make the contours of the relative probability distribution of the GRBs in the  $\log L - \log(1 + z)$  plane. The result is also shown in Figure 4, confidently suggesting a good consistency between our our results



and observations.

The  $\theta_j$ –known sample has 77 GRBs. We randomly pick up a sub-sample of 77 GRBs from our mock GRB sample and show the 1- and 2-dimensional  $\log \theta_j - \log(1+z)$  GRB distributions in Figure 5. The K-S test probabilities are also marked in each panel in the figure. The K-S test yields a global K-S probability larger than 0.1, indicating a good consistency between the mock and observed BAT samples. As described in §3, there is no any intrinsic relation between  $\theta_j$  and  $z$  in our model. The observed  $\theta_j - z$  dependence in the mock sample definitely is due to instrumental selection effects. Therefore, the apparent  $\theta_j - z$  dependence observed in the current GRB sample would be explained with the instrumental selection effect.

As shown in Figure (3a), both  $\theta_c$  and  $L_c$  are degenerate. The triggered GRB number with an instrument in a given operation period may place constraint on the  $\theta_c$  and  $L_c$ , if the local GRB rate is known. However, the  $\rho_0$  is quite uncertain. It is reported that  $\rho_0 \sim 1 \text{ Gpc}^{-3}\text{yr}^{-1}$  (Schmidt 2001; Lloyd-Ronning et al. 2004; Guetta et al. 2005; Liang et al. 2007; Wanderman & Piran 2010). Please note that this rate is obtained without considering the jet collimation. Assuming a typical  $\theta_j$  of 0.1 rad, the  $\rho_0$  is  $\rho_0 \sim 180 \text{ Gpc}^{-3}\text{yr}^{-1}$ . The local Ib/c SN rate, which is reported as  $4.8 \times 10^4 \text{ Gpc}^{-3}\text{yr}^{-1}$  (Marzke et al. 1998; Cappellaro et al. 1999; Folkes et al. 1999), presents a robust upper limit to  $\rho_0$ . BAT triggered 670 GRBs in during 6.5 operation years. We therefore calculate  $\rho_0$  with equation 15 using the best parameter sets derived above. We get  $\rho_0 = 2.85 \times 10^2 \text{ Gpc}^{-3}\text{yr}^{-1}$  for the parameter set  $(\log L_c/\text{erg s}^{-1}, \log \theta_c/\text{rad}) = (49.69, -1.27)$ . The derived local GRB rates are higher than that reported in literature, but still under the local Ib/c SN rate. Our results suggest that  $\sim 0.59\%$  of Type Ib/c SNe may be accompanied by a GRB. This may has profound implications for understanding the relation between GRBs and Type Ib/c SNe (e.g., Lamb et al. 2005).

#### 4. Conclusions and Discussion

Assuming that the intrinsic distributions of both  $L_\gamma$  and  $\theta_j$  are Gaussian, we have shown that the observed  $\theta_j$  dependence on redshift can be interpreted with the instrumental selection effects.

The  $L_\gamma$  (or  $E_\gamma$ ) and  $\theta_j$  are two basic characteristics of the GRB jets. As shown in Figure 1, the observed distributions of  $\theta_j$  and  $E_\gamma$  are log-normal. Frail et al. (2001) proposed the idea of a standard energy reservoir in GRB jets based on the narrow distribution of  $E_\gamma$  (see also Berger et al. 2003). Although our  $E_\gamma$  distribution is still log-normal, the width of the

distribution is much larger than that reported by Frail et al. (2001). Physically, it is difficult to access the intrinsic distributions of both  $L_\gamma$  and  $\theta_j$  from observations since the observed GRB sample with redshift measurement is heavily suffered from instrumental selection effects and observational biases (e.g., Bloom 2003). It was suggested that the intrinsic distributions of  $L_\gamma$  and  $\theta_j$  are a power-law or a broken power-law (e.g., Lin et al. 2004). As shown by Qin et al. (2010), in case of a smooth broken power-law of isotropic peak luminosity  $L$  bootstrap analysis can well reproduce the observed  $L - z$  distributions in both the one- and two-dimensional planes. Intuitively, being due to both instrumental flux-limit and low triggered probability for low  $L_\gamma$ , the trigger probability for GRBs at low  $L_\gamma$  end would be reduced significantly. Similarly, the probability of a narrower jet pointing to the light of sight would be significantly lowered. Hence its detection probability would rapidly drop. Therefore, observationally, one cannot distinguish a Gaussian or a power-law distribution for with current GRB samples. In order to examine this expectation, we take the distributions of  $L_\gamma$  and  $\theta_j$  as a power-law function, e.g.,  $\Phi(L_\gamma) = (L_\gamma/L_c^{\text{PL}})^{\kappa_L}$ ;  $\psi(\theta_j) = (\theta_j/\theta_c^{\text{PL}})^{\kappa_\theta}$ . We fix  $L_c^{\text{PL}} = 10^{50} \text{erg s}^{-1}$  and  $\theta_c^{\text{PL}} = 0.1 \text{ rad}$ , but let  $\kappa_L$  and  $\kappa_\theta$  as free parameters. Our bootstrapping method still can well reproduce the observations. The contours of the relative  $P_{K-S}^G$  in the  $\kappa_L - \kappa_\theta$  plane are also plotted in Figure (3b) for comparison with the  $P_{K-S}^G$  distribution in the  $\theta_c - L_c$  plane. Similarly,  $\kappa_L$  and  $\kappa_\theta$  seem to be degenerated as that of  $\theta_c$  and  $L_c$ . In case of  $\kappa_\theta \propto \kappa_L^{0.5}$ , our results roughly reproduce the observations. The parameter set  $(\kappa_L, \kappa_\theta) = (-1.02, -1.42)$  gives the best consistency between our results and the BAT GRB sample, which is shown in Figs. 6 and 7. Yonetoku et al. (2005) suggested a  $\kappa$  of  $\sim -2$  from *CGRO/BATSE* data, which is steeper than our result for the BAT sample. The derived  $\rho_0$  in the parameter set  $(\kappa_L, \kappa_\theta) = (-1.02, -1.42)$  is  $1.52 \times 10^2 \text{ Gpc}^{-3} \text{yr}^{-1}$ .

Some apparent correlations between some GRB properties and redshift were discussed by some authors with small samples, such as the redshift dependence of the spectral lag of GRBs in prompt phases (Yi et al. 2008) and the duration of the shallow decay phase of GRB X-ray afterglows (Stratta et al. 2009). Physically, these correlations may be results from the cosmic evolution of the explosion energy and/or the jet geometry (e.g., Xu et al. 2005), if they are intrinsic. However, as shown in our analysis, there are no convincing cosmic evolution features. Therefore, these apparent correlations may be, at least partially, due to sample selection effects or observational biases.

Tight correlations between  $E_\gamma$  and  $E_p'$  (Ghirlanda relation; Ghirlanda et al. 2004) or among  $E_{\text{iso}}$ ,  $t_j$  and  $E_p'$  (Liang-Zhang relation, Liang & Zhang 2005) were discovered with small GRB sample. As shown in this analysis, the  $E_\gamma$  distribution would suffer great selection effects. It is known that the observed distribution of  $E_p$  is also due to the selection effect. The observed narrow distribution of  $E_p$  by *CGRO/BATSE* is significantly broadened by the observations with *HETE-2* and *BAT*. Our analysis cannot figure out if the selections effects

on both  $E_\gamma$  and  $E_p$  distributions can be canceled out and evaluates whether these relations are intrinsic.

We acknowledge the use of the public data from the Swift data archive. We thank helpful discussion with Bing Zhang, X. F. Wu, and Shuang-Nan Zhang. This work is supported by the National Natural Science Foundation of China under grants No. 11063001, 10873002 and 11025313, the National Basic Research Program (“973” Program) of China (Grant 2009CB824800), Special Foundation for Distinguished Expert Program of Guangxi, the Guangxi SHI-BAI-QIAN project (Grant 2007201), the Guangxi Natural Science Foundation (2010GXNSFA013112 and 2010GXNSFC013011), the special funding for national outstanding young scientist (Contract No. 2011-135), and the 3th Innovation Project of Guangxi University.

## REFERENCES

- Amati, L., Frontera, F., Vietri, M., et al. 2000, *Science*, 290, 953
- Andersen, M. I., Masi, G., Jensen, B. L., & Hjorth, J. 2003, *GRB Coordinates Network*, 1993, 1
- Band, D., Matteson, J., Ford, L., et al. 1993, *ApJ*, 413, 281
- Band, D. L. 2006, *ApJ*, 644, 378
- Barth, A. J., Sari, R., Cohen, M. H., et al. 2003, *ApJ*, 584, L47
- Berger, E., Diercks, A., Frail, D. A., et al. 2001, *ApJ*, 556, 556
- Berger, E., Gladders, M., & Oemler, G. 2005, *GRB Coordinates Network*, 3201, 1
- Berger, E., Kulkarni, S. R., & Frail, D. A. 2003, *ApJ*, 590, 379
- Berger, E., Sari, R., Frail, D. A., et al. 2000, *ApJ*, 545, 56
- Bissaldi, E. 2009, *GRB Coordinates Network*, 9933, 1
- Bissaldi, E., & Connaughton, V. 2009, *GRB Coordinates Network*, 9866, 1
- Bloom, J. S. 2003, *AJ*, 125, 2865
- Bloom, J. S., Djorgovski, S. G., Kulkarni, S. R., & Frail, D. A. 1998, *ApJ*, 507, L25

- Bloom, J. S., Frail, D. A., & Sari, R. 2001, *AJ*, 121, 2879
- Bromm, V., & Loeb, A. 2002, *ApJ*, 575, 111
- Butler, N. R., Bloom, J. S., & Poznanski, D. 2010, *ApJ*, 711, 495
- Butler, N. R., Kocevski, D., Bloom, J. S., & Curtis, J. L. 2007, *ApJ*, 671, 656
- Cappellaro, E., Evans, R., & Turatto, M. 1999, *A&A*, 351, 459
- Castro, S. M., Diercks, A., Djorgovski, S. G., et al. 2000, *GRB Coordinates Network*, 605, 1
- Castro, S. M., Djorgovski, S. G., Kulkarni, S. R., et al. 2000, *GRB Coordinates Network*, 851, 1
- Cenko, S. B., Frail, D. A., Harrison, F. A., et al. 2011, *ApJ*, 732, 29
- Cenko, S. B., Kasliwal, M., Harrison, F. A., et al. 2006, *ApJ*, 652, 490
- Chapman, R., Tanvir, N. R., Priddey, R. S., & Levan, A. J. 2007, *MNRAS*, 382, L21
- Chevalier, R. A., & Li, Z.-Y. 2000, *ApJ*, 536, 195
- Covino, S., Capalbi, M., Perri, M., Mangano, V., & Burrows, D. N. 2005, *GRB Coordinates Network*, 3508, 1
- Cucchiara, A., Levan, A. J., Fox, D. B., et al. 2011, *ApJ*, 736, 7
- Curran, P. A., van der Horst, A. J., Wijers, R. A. M. J., et al. 2007, *MNRAS*, 381, L65
- Dai, Z. G., Liang, E. W., & Xu, D. 2004, *ApJ*, 612, L101
- Daigne, F., Rossi, E. M., & Mochkovitch, R. 2006, *MNRAS*, 372, 1034
- Djorgovski, S. G., Frail, D. A., Kulkarni, S. R., et al. 2001, *ApJ*, 562, 654
- Djorgovski, S. G., Kulkarni, S. R., Bloom, J. S., et al. 1998, *ApJ*, 508, L17
- Endo, Y., Tashiro, M., Abe, K., et al. 2005, *GRB Coordinates Network*, 4393, 1
- Fenimore, E. E., Palmer, D., Galassi, M., et al. 2003, *Gamma-Ray Burst and Afterglow Astronomy 2001: A Workshop Celebrating the First Year of the HETE Mission*, 662, 491
- Ferrero, P., Klose, S., Kann, D. A., et al. 2009, *A&A*, 497, 729

- Firmani, C., Avila-Reese, V., Ghisellini, G., & Tutukov, A. V. 2004, *ApJ*, 611, 1033
- Folkes, S., Ronen, S., Price, I., et al. 1999, *MNRAS*, 308, 459
- Frail, D. A., Kulkarni, S. R., Sari, R., et al. 2001, *ApJ*, 562, L55
- Frail, D. A., Waxman, E., & Kulkarni, S. R. 2000, *ApJ*, 537, 191
- Frail, D. A., Yost, S. A., Berger, E., et al. 2003, *ApJ*, 590, 992
- Frontera, F., Amati, L., Guidorzi, C., et al. 2002, *GRB Coordinates Network*, 1215, 1
- Fynbo, J. P. U., Jakobsson, P., Prochaska, J. X., et al. 2009, *ApJS*, 185, 526
- Galama, T. J., Reichart, D., Brown, T. M., et al. 2003, *ApJ*, 587, 135
- Gehrels, N., Chincarini, G., Giommi, P., et al. 2004, *ApJ*, 611, 1005
- Ghirlanda, G., Ghisellini, G., & Lazzati, D. 2004, *ApJ*, 616, 331
- Ghirlanda, G., Ghisellini, G., Lazzati, D., & Firmani, C. 2004, *ApJ*, 613, L13
- Golenetskii, S., Aptekar, R., Mazets, E., et al. 2009, *GRB Coordinates Network*, 9030, 1
- Guetta, D., Piran, T., & Waxman, E. 2005, *ApJ*, 619, 412
- Halpern, J. P., Uglesich, R., Mirabal, N., et al. 2000, *ApJ*, 543, 697
- Harrison, F. A., Bloom, J. S., Frail, D. A., et al. 1999, *ApJ*, 523, L121
- Harrison, F. A., Yost, S. A., Sari, R., et al. 2001, *ApJ*, 559, 123
- Holland, S. T., Soszyński, I., Gladders, M. D., et al. 2002, *AJ*, 124, 639
- Hopkins, A. M., & Beacom, J. F. 2006, *ApJ*, 651, 142
- Hurley, K., Cline, T., Mazets, E., et al. 2002, *GRB Coordinates Network*, 1483, 1
- in't Zand, J. J. M., Kuiper, L., Amati, L., et al. 2001, *ApJ*, 559, 710
- Jakobsson, P., Hjorth, J., Fynbo, J. P. U., et al. 2004, *A&A*, 427, 785
- Kaneko, Y., Preece, R. D., Briggs, M. S., et al. 2006, *ApJS*, 166, 298
- Kann, D. A., Laux, U., Filgas, R., et al. 2007, *GRB Coordinates Network*, 6935, 1

- Kistler, M. D., Yüksel, H., Beacom, J. F., Hopkins, A. M., & Wyithe, J. S. B. 2009, *ApJ*, 705, L104
- Kistler, M. D., Yüksel, H., Beacom, J. F., & Stanek, K. Z. 2008, *ApJ*, 673, L119
- Klose, S., Greiner, J., Rau, A., et al. 2004, *AJ*, 128, 1942
- Kocevski, D., & Liang, E. 2006, *ApJ*, 642, 371
- Krimm, H. A., Granot, J., Marshall, F. E., et al. 2007, *ApJ*, 665, 554
- Kulkarni, S. R., Djorgovski, S. G., Odewahn, S. C., et al. 1999, *Nature*, 398, 389
- Lamb, D., Ricker, G., Atteia, J.-L., et al. 2002, *GRB Coordinates Network*, 1600, 1
- Lamb, D. Q., Donaghy, T. Q., & Graziani, C. 2005, *ApJ*, 620, 355
- Langer, N., & Norman, C. A. 2006, *ApJ*, 638, L63
- Le Floch, E., Duc, P.-A., Mirabel, I. F., et al. 2002, *ApJ*, 581, L81
- Li, L.-X. 2008, *MNRAS*, 388, 1487
- Liang, E. W., Dai, Z. G., & Wu, X. F. 2004, *ApJ*, 606, L29
- Liang, E.-W., Racusin, J. L., Zhang, B., Zhang, B.-B., & Burrows, D. N. 2008, *ApJ*, 675, 528
- Liang, E., & Zhang, B. 2005, *ApJ*, 633, 611
- Liang, E., Zhang, B., Virgili, F., & Dai, Z. G. 2007, *ApJ*, 662, 1111
- Lin, J. R., Zhang, S. N., & Li, T. P. 2004, *ApJ*, 605, 819
- Lloyd-Ronning, N. M., Fryer, C. L., & Ramirez-Ruiz, E. 2002, *ApJ*, 574, 554
- Malesani, D., Goldoni, P., Fynbo, J. P. U., et al. 2009, *GRB Coordinates Network*, 9942, 1
- Marzke, R. O., da Costa, L. N., Pellegrini, P. S., Willmer, C. N. A., & Geller, M. J. 1998, *ApJ*, 503, 617
- Masetti, N., Palazzi, E., Pian, E., et al. 2000, *A&A*, 354, 473
- Matheson, T., Garnavich, P. M., Foltz, C., et al. 2003, *ApJ*, 582, L5

- Matsubayashi, T., Yamazaki, R., Yonetoku, D., Murakami, T., & Ebisuzaki, T. 2005, *Progress of Theoretical Physics*, 114, 983
- Mirabal, N., Halpern, J. P., Kulkarni, S. R., et al. 2002, *ApJ*, 578, 818
- Nava, L., Ghirlanda, G., Ghisellini, G., & Firmani, C. 2008, *MNRAS*, 391, 639
- Paczynski, B. 1998, *ApJ*, 494, L45
- Pandey, S. B., Sahu, D. K., Resmi, L., et al. 2003, *Bulletin of the Astronomical Society of India*, 31, 19
- Pandey, S. B., Swenson, C. A., Perley, D. A., et al. 2010, *ApJ*, 714, 799
- Piran, T., Jimenez, R., & Band, D. 2000, *Gamma-ray Bursts*, 5th Huntsville Symposium, 526, 87
- Preece, R. D., Briggs, M. S., Mallozzi, R. S., et al. 2000, *ApJS*, 126, 19
- Price, P. A., Harrison, F. A., Galama, T. J., et al. 2001, *ApJ*, 549, L7
- Price, P. A., Kulkarni, S. R., Berger, E., et al. 2002, *ApJ*, 571, L121
- Price, P. A., Kulkarni, S. R., Berger, E., et al. 2003, *ApJ*, 589, 838
- Price, P. A., Kulkarni, S. R., Schmidt, B. P., et al. 2003, *ApJ*, 584, 931
- Qin, S.-F., Liang, E.-W., Lu, R.-J., Wei, J.-Y., & Zhang, S.-N. 2010, *MNRAS*, 406, 558
- Racusin, J., Kennea, J., Fox, D., et al. 2005, *GRB Coordinates Network*, 4169, 1
- Racusin, J. L., & Burrows, D. N. 2008, *American Institute of Physics Conference Series*, 1065, 245
- Racusin, J. L., Liang, E. W., Burrows, D. N., et al. 2009, *ApJ*, 698, 43
- Racusin, J. L., & Burrows, D. N. 2010, *Bulletin of the American Astronomical Society*, 36, #603.08
- Rau, A., Connaughton, V., & Briggs, M. 2009, *GRB Coordinates Network*, 9057, 1
- Rhoads, J. E. 1997, *ApJ*, 487, L1
- Ricker, G., Hurley, K., Lamb, D., et al. 2002, *ApJ*, 571, L127
- Rowan-Robinson, M. 1999, *Ap&SS*, 266, 291

- Sakamoto, T., Barthelmy, S. D., Barbier, L., et al. 2008, *ApJS*, 175, 179
- Sakamoto, T., Barthelmy, S. D., Baumgartner, W. H., et al. 2011, *ApJS*, 195, 2
- Sakamoto, T., Ricker, G., Atteia, J.-L., et al. 2005, *GRB Coordinates Network*, 3189, 1
- Sakamoto, T., Sato, G., Barbier, L., et al. 2009, *ApJ*, 693, 922
- Salvatterra, R., Campana, S., Chincarini, G., et al. 2008, *IAU Symposium*, 255, 212
- Salvatterra, R., Campana, S., Chincarini, G., Covino, S., & Tagliaferri, G. 2008, *MNRAS*, 385, 189
- Salvatterra, R., Guidorzi, C., Campana, S., Chincarini, G., & Tagliaferri, G. 2009, *MNRAS*, 396, 299
- Sari, R., Piran, T., & Halpern, J. P. 1999, *ApJ*, 519, L17
- Schmidt, M. 2001, *ApJ*, 552, 36
- Soderberg, A. M., Kulkarni, S. R., Berger, E., et al. 2004, *Nature*, 430, 648
- Stanek, K. Z., Garnavich, P. M., Nutzman, P. A., et al. 2005, *ApJ*, 626, L5
- Stratta, G., Guetta, D., D’Elia, V., et al. 2009, *A&A*, 494, L9
- Tagliaferri, G., Antonelli, L. A., Chincarini, G., et al. 2005, *A&A*, 443, L1
- Tanvir, N., Levan, A., Wiersema, K., et al. 2009, *GRB Coordinates Network*, 9219, 1
- Thöne, C. C., Kann, D. A., Jóhannesson, G., et al. 2010, *A&A*, 523, A70
- Tinney, C., Stathakis, R., Cannon, R., & Galama, T. 1998, *IAU Circ.*, 6896, 3
- Totani, T. 1997, *ApJ*, 486, L71
- Virgili, F. J., Zhang, B., Nagamine, K., & Choi, J.-H. 2011, *arXiv:1105.4650*
- Vreeswijk, P. M., Fruchter, A., Kaper, L., et al. 2001, *ApJ*, 546, 672
- Vreeswijk, P. M., Rol, E., Hjorth, J., et al. 1999, *GRB Coordinates Network*, 496, 1
- Wanderman, D., & Piran, T. 2010, *MNRAS*, 406, 1944
- Wang, F. Y., & Dai, Z. G. 2009, *MNRAS*, 400, L10
- Wei, D. M., & Gao, W. H. 2003, *MNRAS*, 345, 743



- Willingale, R., Osborne, J. P., O'Brien, P. T., et al. 2004, MNRAS, 349, 31
- Xu, L., Wu, X. F., & Dai, Z. G. 2005, ApJ, 634, 1155
- Yüksel, H., & Kistler, M. D. 2007, Phys. Rev. D, 75, 083004
- Yi, T.-F., Xie, G.-Z., & Zhang, F.-W. 2008, Chinese J. Astron. Astrophys., 8, 81
- Yonetoku, D., Murakami, T., Nakamura, T., et al. 2004, ApJ, 609, 935
- Yonetoku, D., Yamazaki, R., Nakamura, T., & Murakami, T. 2005, MNRAS, 362, 1114
- Zhang, B., Kobayashi, S., Mészáros, P., Lloyd-Ronning, N. M., & Dai, X. 2004, Gamma-Ray Bursts: 30 Years of Discovery, 727, 208
- Zhang, B., & Mészáros, P. 2004, International Journal of Modern Physics A, 19, 2385
- Zhang, B., Zhang, B.-B., Liang, E.-W., et al. 2007, ApJ, 655, L25

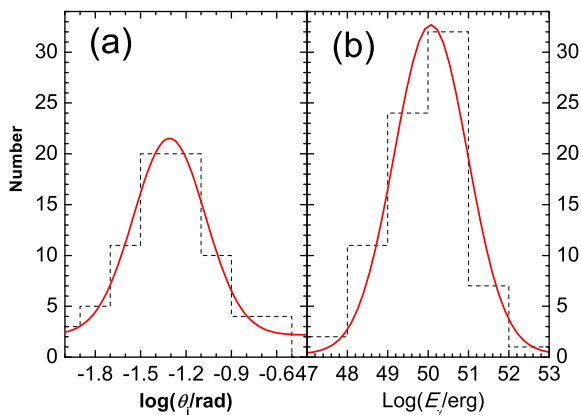


Fig. 1.— Distributions of the jet opening angle (panel a) and the geometrically-corrected gamma-ray energy  $E_\gamma$  (panel b) for the 77 GRBs in Table 1. The solid lines are the best fits to the data with a Gaussian function.

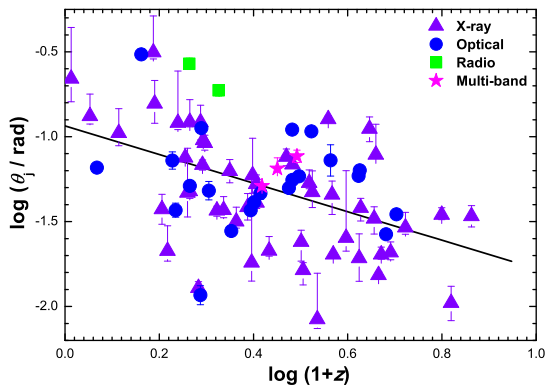


Fig. 2.— Jet opening angles as a function of redshift for the 77 GRBs in Table 1. The GRBs with  $t_j$  measuring at different bands are marked with different symbols as indicating in the legend. The solid line is the best fit to all data.

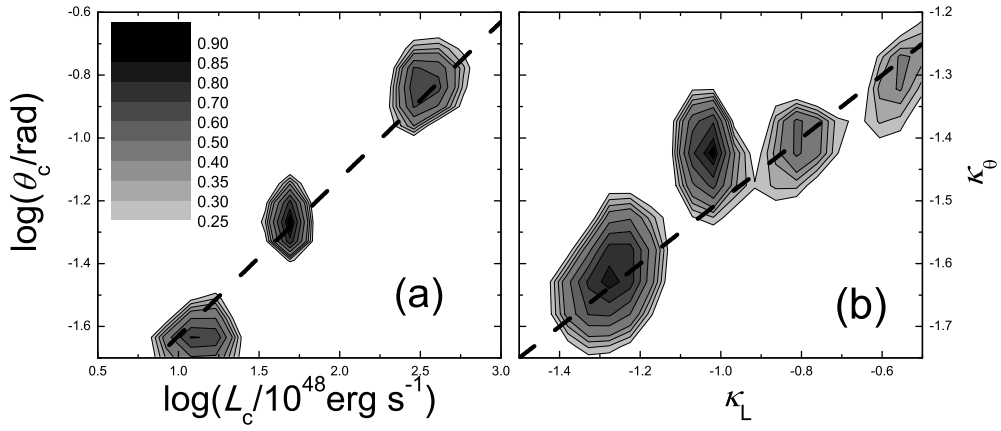


Fig. 3.— Contours of the global K-S test probability in the  $L_c - \theta_c$  plane (panel a) and  $\kappa_L - \kappa_\theta$  plane (panel b). The dash lines denote  $\theta_c \propto L_c^{0.5}$  and  $\kappa_\theta \propto \kappa_L^{0.5}$ , respectively.

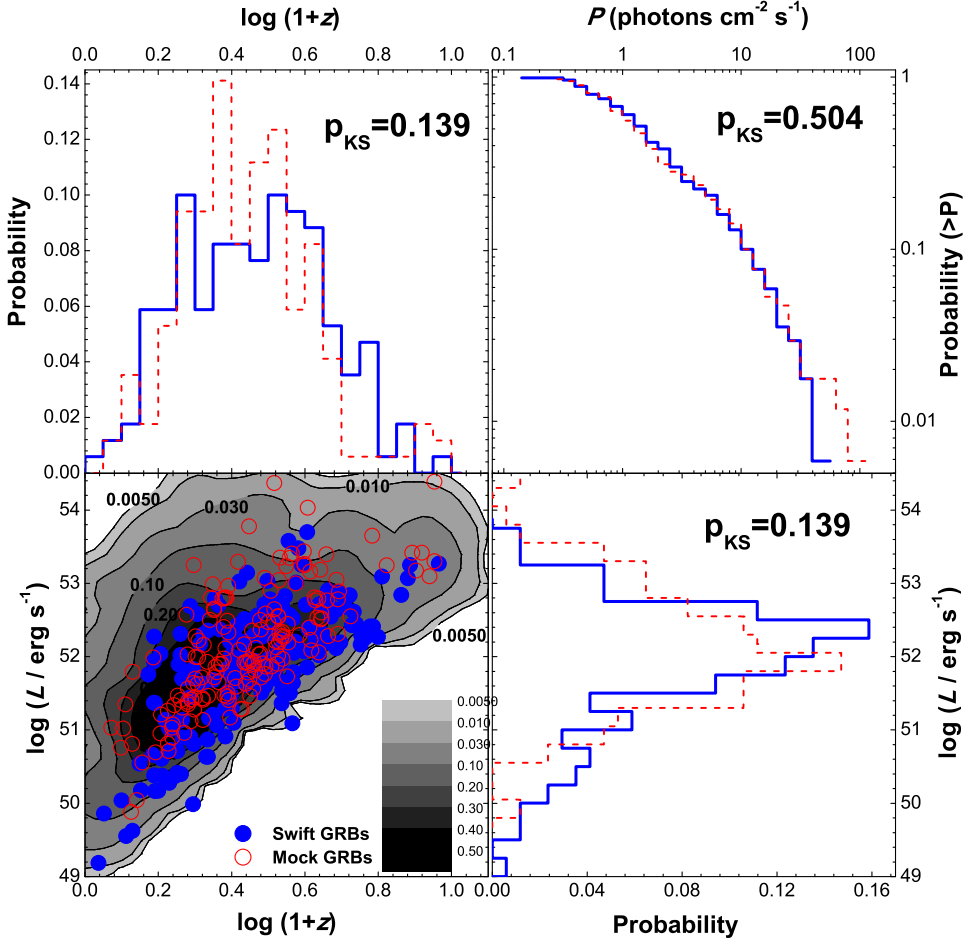


Fig. 4.— Comparisons of two-dimensional  $\log L$ - $\log(1+z)$  distributions and one-dimensional  $\log L$ ,  $\log(1+z)$  and  $\log P$  (accumulative  $\log N$ - $\log P$ ) distributions between the 170 Swift GRBs (solid dots and solid lines) and our results (open dots and dashed lines). The contours in the  $\log L$ - $\log(1+z)$  plane show the normalized probability distributions of the mock GRBs with different color scale lines. One dimensional K-S test probabilities for the comparisons are marked in each panel.

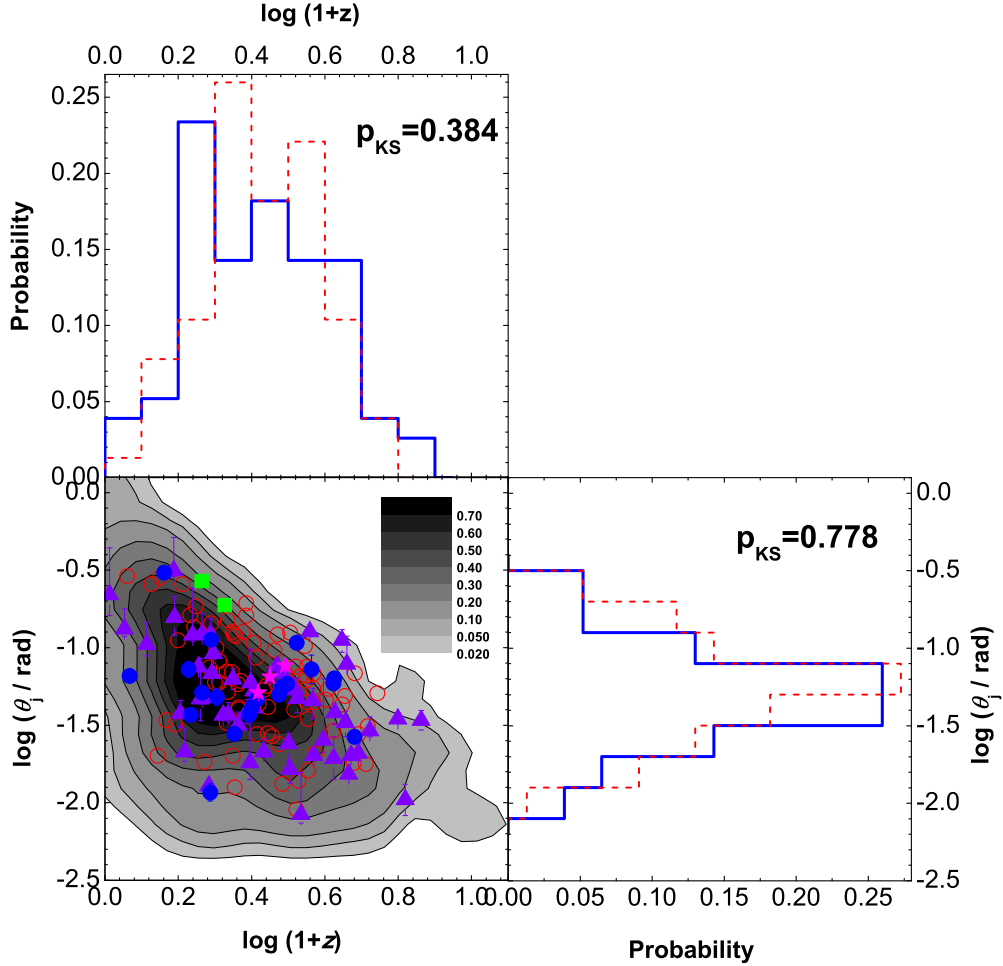


Fig. 5.— Comparisons of two-dimensional  $\log\theta_j$ - $\log(1+z)$  distributions and one-dimensional  $\log\theta_j$  and  $\log(1+z)$  distributions between the 77 GRBs with opening angles (solid lines) and our results (open dots and dashed lines). The contours in the  $\log\theta_j$ - $\log(1+z)$  plane show the normalized probability distributions of the mock GRBs with different color scale lines. One dimensional K-S test probabilities for the comparisons are marked in each panel. Other symbols in the  $\log\theta_j$ - $\log(1+z)$  plane are the same as in Fig. (2)

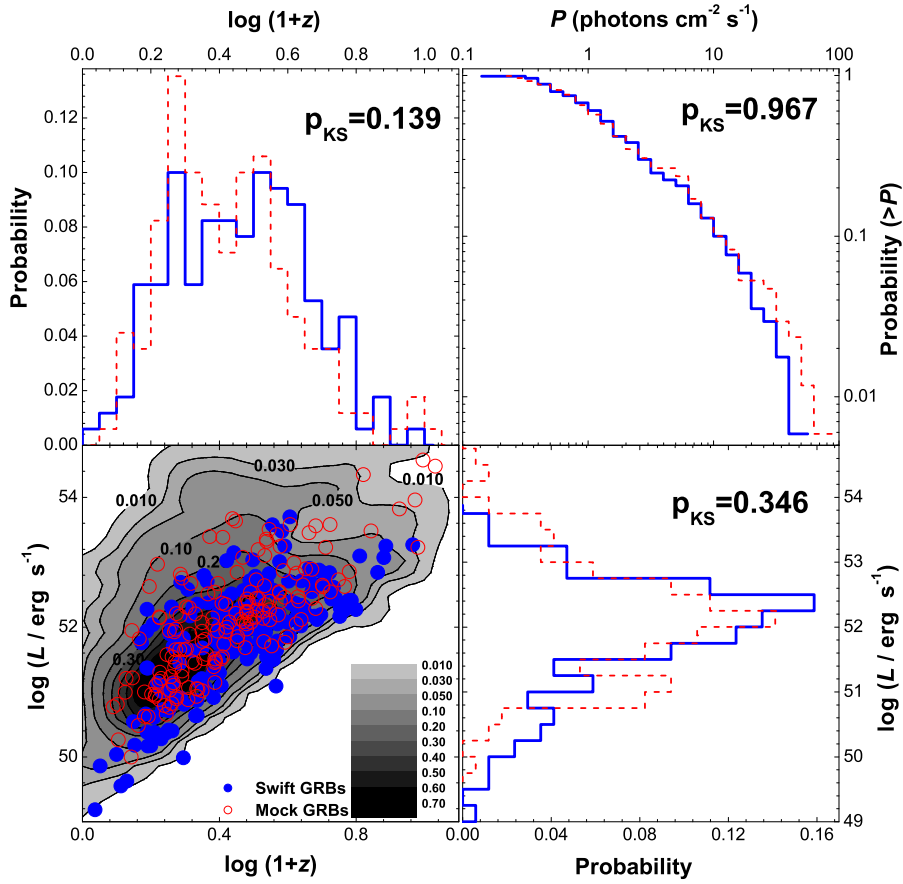


Fig. 6.— The same as Fig 4 but for power law distributions of the jet-corrected luminosity and jet opening angle.

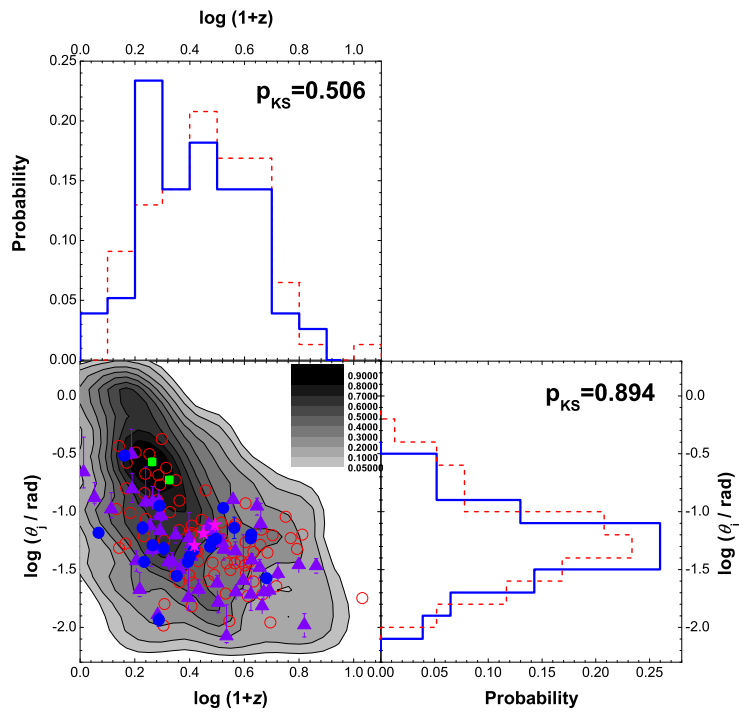


Fig. 7.— The same as Fig 5 but for the power law distributions of the jet-corrected luminosity and jet opening angle.

Table 1. Jet Break Times and Jet Opening Angles

GRB	$z$	$S_\gamma$ ( $10^{-6}$ erg $\text{cm}^{-2}$ )	Energy <sup>a</sup> (keV)	$E_{\text{iso}}(\gamma)^b$ ( $10^{51}$ erg)	$t_j$ (days)	Band <sup>c</sup>	$\theta_j^d$ (rad)	$E_\gamma^e$ ( $10^{51}$ erg)	Refs.
970508	0.835	3.17	20-2000	8.25	25±5	R	0.269±0.020	0.296	1,2,3
970828	0.958	96.00	20-2000	272	2.2±0.4	X	0.068±0.005	0.631	4,2,4
980703	0.966	22.60	20-2000	67.2	3.4±0.5	X	0.095±0.005	0.306	5,2,6
990123	1.60	268.00	20-2000	1945	2.04±0.46	O	0.047±0.004	2.11	7,2,7
990510	1.619	22.60	20-2000	182	1.20±0.08	O/R	0.051±0.001	0.239	8,2,9
990705	0.84	93.00±2.00	40-700	298	1.0±0.2	O	0.051±0.004	0.393	10,11,12
991216	1.02	194.00	20-2000	655	1.2±0.4	O	0.048±0.006	0.756	13,2,14
000301C	2.034	4.10	25-1000	57.7	7.3±0.5	O	0.11±0.003	0.349	15,16,16
000418	1.119	20.00	15-1000	95.3	25±5	R	0.188±0.014	1.67	17,18,18
000926	2.037	6.20	25-100	200	1.8±0.1	O	0.056±0.001	0.310	19,20,21
010222	1.477	120.00±3.00	2-700	1383	0.93 <sup>+0.15</sup> <sub>-0.06</sub>	O	0.037 <sup>+0.002</sup> <sub>-0.0009</sub>	0.940	22,23,24
010921	0.451	15.40±0.20	8-400	13.8	33.0±6.5	O	0.306±0.023	0.638	25,26,27
011211	2.14	5.00	40-700	117	1.77±0.28	O	0.058±0.004	0.199	28,29,30
020124	3.2	6.10	30-400	227	3.0±0.4	O	0.059±0.003	0.392	31,31,32
020405	0.69	38.00±4.00	50-700	114	1.67±0.52	O	0.072±0.009	0.299	25,33,30
020813	1.254	38.00	25-100	1701	0.43±0.06	O	0.028±0.002	0.661	34,35,34
021004	2.332	3.20	7-400	58.9	7.6±0.3	O	0.108±0.002	0.341	36,37,38
030226	1.986	5.70	30-400	98.9	1.04±0.12	O	0.050±0.002	0.123	39,39,39
030328	1.52	29.00	30-400	350	0.8±0.1	O	0.041±0.002	0.295	31,31,40
030329	0.168	120.00	30-400	16.8	0.47±0.005	O	0.066±0.0009	0.036	41,41,41
030429	2.66	0.38	30-400	13.2	1.77±1.0	O	0.073±0.015	0.035	31,31,42
041006	0.716	7.00	30-400	21.0	0.16±0.04	O	0.037±0.003	0.014	29,29,43
050315	1.95	3.22±0.146	15-150	67.4	2.78 <sup>+0.80</sup> <sub>-0.88</sub>	X	0.076 <sup>+0.008</sup> <sub>-0.009</sub>	0.195	44,44,45
050318	1.44	1.08±0.077	15-150	17.6	0.24 <sup>+0.12</sup> <sub>-0.11</sub>	X	0.038±0.007	0.013	44,44,45
050319	3.24	1.9 <sup>+0.2</sup> <sub>-0.3</sub>	15-350	69.6	0.64 <sup>+0.22</sup> <sub>-0.30</sub>	X	0.038 <sup>+0.005</sup> <sub>-0.007</sub>	0.050	46,46,45
050408	1.236	1.4	2-30	89.9	1.39±0.58	X	0.063±0.01	0.177	47,48,49
050416A	0.65	0.37±0.04	15-150	0.991	0.01 <sup>+0.01</sup> <sub>-0.005</sub>	X	0.021 <sup>+0.007</sup> <sub>-0.0003</sub>	0.0002	44,44,45
050505	4.28	2.49±0.18	15-150	174	0.53 <sup>+0.29</sup> <sub>-0.13</sub>	X	0.029 <sup>+0.006</sup> <sub>-0.003</sub>	0.074	44,44,45
050525A	0.606	15.30±0.22	15-150	22.6	0.16±0.09	X	0.037±0.008	0.016	44,44,50
050802	1.71	2.00±0.16	15-150	37.0	0.07 <sup>+0.04</sup> <sub>-0.01</sub>	X	0.021 <sup>+0.004</sup> <sub>-0.002</sub>	0.008	44,44,45
050814	5.3	2.01±0.22	15-150	184	1.03 <sup>+0.26</sup> <sub>-0.18</sub>	X	0.035 <sup>+0.003</sup> <sub>-0.002</sub>	0.111	44,44,45
050820A	2.62	3.44±0.24	15-150	163	18±2	X	0.127±0.005	1.31	44,44,51
050826	0.3	0.41±0.07	15-150	0.242	0.45 <sup>+0.39</sup> <sub>-0.20</sub>	X	0.105 <sup>+0.035</sup> <sub>-0.018</sub>	0.001	44,44,45
050904	6.29	5.40±0.20	15-150	2267	2.6±1	O	0.034±0.005	1.31	52,52,52
050922C	2.2	1.62±0.05	15-150	56.5	0.05 <sup>+0.01</sup> <sub>-0.03</sub>	X	0.016 <sup>+0.002</sup> <sub>-0.003</sub>	0.008	44,44,45
051016B	0.94	0.17±0.02	15-150	0.969	1.56 <sup>+0.96</sup> <sub>-1.00</sub>	X	0.122 <sup>+0.028</sup> <sub>-0.029</sub>	0.007	44,44,45
051022	0.8	160	2-400	362	2.9±0.2	X	0.075±0.002	1.02	53,53,53
051109A	2.35	2.20±0.27	15-150	75.9	0.92 <sup>+0.71</sup> <sub>-0.51</sub>	X	0.047 <sup>+0.014</sup> <sub>-0.001</sub>	0.084	44,44,45
051111	1.55	4.08±0.13	15-150	81.4	0.49 <sup>+0.16</sup> <sub>-0.10</sub>	X	0.041 <sup>+0.005</sup> <sub>-0.003</sub>	0.068	44,44,45
051221A	0.55	2.40±0.40	100-2000	4.46	4.07 <sup>+3.40</sup> <sub>-2.88</sub>	X	0.157 <sup>+0.049</sup> <sub>-0.042</sub>	0.055	44,54,45
060115	3.53	1.71±0.15	15-150	92.3	0.51 <sup>+0.22</sup> <sub>-0.28</sub>	X	0.033 <sup>+0.005</sup> <sub>-0.007</sub>	0.050	44,44,45
060124	2.3	0.48±0.03	15-350	11.9	0.68 <sup>+0.32</sup> <sub>-0.14</sub>	X	0.053 <sup>+0.009</sup> <sub>-0.004</sub>	0.017	44,46,45
060206	4.05	0.83±0.04	15-150	57.9	0.57±0.06	O	0.035±0.001	0.035	44,44,55
060210	3.91	7.66±0.41	15-150	569	0.30 <sup>+0.11</sup> <sub>-0.08</sub>	X	0.021 <sup>+0.003</sup> <sub>-0.002</sub>	0.123	44,44,45
060218	0.03	1.57±0.15	15-150	0.008	0.82 <sup>+1.53</sup> <sub>-0.69</sub>	X	0.220 <sup>+0.153</sup> <sub>-0.069</sub>	0.0002	44,44,45
060418	1.49	8.33±0.25	15-150	144	0.07 <sup>+0.20</sup> <sub>-0.04</sub>	X	0.018 <sup>+0.020</sup> <sub>-0.005</sub>	0.024	44,44,45
060526	3.22	1.26±0.15	15-150	63.7	2.41±0.06	O	0.063±0.001	0.128	44,44,56
060605	3.8	0.70±0.09	15-150	43.6	0.24±0.02	O	0.027±0.001	0.016	44,44,57
060614	0.13	28.20±0.40	15-350	2.04	1.45 <sup>+1.16</sup> <sub>-0.41</sub>	X	0.132 <sup>+0.040</sup> <sub>-0.014</sub>	0.018	44,46,45
060707	3.43	1.60±0.15	15-150	79.9	12.26 <sup>+5.25</sup> <sub>-5.72</sub>	X	0.111 <sup>+0.018</sup> <sub>-0.020</sub>	0.495	44,44,45
060714	2.71	2.83±0.17	15-150	109	0.12±0.01	X	0.020±0.001	0.022	44,44,58
060729	0.54	2.61±0.21	15-150	4.70	26.23 <sup>+34.61</sup> <sub>-6.12</sub>	X	0.314 <sup>+0.155</sup> <sub>-0.028</sub>	0.229	44,44,45
060814	0.84	14.60±0.24	15-150	88.7	0.55±0.14	X	0.048±0.005	0.101	44,44,45
060906	3.69	2.21±0.14	15-150	138	0.16 <sup>+0.04</sup> <sub>-0.03</sub>	X	0.020 <sup>+0.002</sup> <sub>-0.001</sub>	0.028	44,44,45
060908	2.43	2.80±0.11	15-150	101	0.01 <sup>+0.02</sup> <sub>-0.003</sub>	X	0.008 <sup>+0.005</sup> <sub>-0.001</sub>	0.004	44,44,45
060926	3.21	0.22±0.03	15-150	11.5	0.06±0.05	X	0.019±0.006	0.002	44,44,45
060927	5.6	1.13±0.07	15-150	119	0.04±0.02	X	0.011±0.002	0.007	44,44,45
061121	1.31	13.70±0.20	15-150	280	0.34 <sup>+0.18</sup> <sub>-0.08</sub>	X	0.032 <sup>+0.006</sup> <sub>-0.003</sub>	0.140	44,44,45
070125	1.547	22.50±3.50	20-10000	108	1.05 <sup>+0.35</sup> <sub>-0.30</sub>	X	0.053 <sup>+0.007</sup> <sub>-0.006</sub>	0.149	59,59,45
070208	1.17	0.45±0.10	15-150	3.66	0.11 <sup>+0.05</sup> <sub>-0.03</sub>	X	0.037 <sup>+0.007</sup> <sub>-0.004</sub>	0.003	44,44,45
070306	1.5	9.00 <sup>+0.50</sup> <sub>-0.80</sub>	15-350	88.8	1.33 <sup>+1.79</sup> <sub>-0.86</sub>	X	0.059 <sup>+0.030</sup> <sub>-0.014</sub>	0.156	44,46,45
070318	0.84	2.48±0.11	15-150	13.2	3.57 <sup>+2.88</sup> <sub>-0.63</sub>	X	0.122 <sup>+0.037</sup> <sub>-0.008</sub>	0.098	44,44,45
070411	2.95	2.70±0.16	15-150	115	0.24 <sup>+0.58</sup> <sub>-0.11</sub>	X	0.025 <sup>+0.023</sup> <sub>-0.005</sub>	0.037	44,44,45
070508	0.82	19.60±0.27	15-150	124	0.58 <sup>+0.93</sup> <sub>-0.50</sub>	X	0.047 <sup>+0.028</sup> <sub>-0.015</sub>	0.136	44,44,45
070611	2.04	0.39±0.06	15-150	9.25	1.13 <sup>+0.39</sup> <sub>-0.53</sub>	X	0.069 <sup>+0.009</sup> <sub>-0.012</sub>	0.022	44,44,45
070714B	0.92	0.72±0.09	15-150	19.2	0.01±0.002	X	0.013±0.001	0.002	44,44,45



Table 1—Continued

GRB	$z$	$S_\gamma$ ( $10^{-6}$ erg cm $^{-2}$ )	Energy <sup>a</sup> (keV)	$E_{\text{iso}}(\gamma)$ <sup>b</sup> ( $10^{51}$ erg)	$t_j$ (days)	Band <sup>c</sup>	$\theta_j^d$ (rad)	$E_\gamma^e$ ( $10^{51}$ erg)	Refs.
070721B	3.63	7.40±0.60	15-350	365	0.11 <sup>+0.01</sup> <sub>-0.02</sub>	X	0.015±0.001	0.043	60,60,45
070810A	2.17	0.69±0.06	15-150	17.3	0.09 <sup>+0.04</sup> <sub>-0.06</sub>	X	0.024 <sup>+0.004</sup> <sub>-0.006</sub>	0.005	44,44,45
071003	1.1	8.30±0.30	15-150	206	0.41 <sup>+0.07</sup> <sub>-0.09</sub>	X	0.037 <sup>+0.002</sup> <sub>-0.003</sub>	0.139	44,44,45
071010A	0.98	0.20±0.04	15-150	1.22	0.81 <sup>+0.22</sup> <sub>-0.20</sub>	X	0.092 <sup>+0.010</sup> <sub>-0.009</sub>	0.005	44,44,45
071010B	0.947	4.40±0.10	15-150	19.1	3.44±0.39	O	0.113±0.005	0.121	44,44,61
071031	2.69	0.90±0.13	15-150	34.3	0.71 <sup>+0.35</sup> <sub>-0.50</sub>	X	0.046 <sup>+0.008</sup> <sub>-0.012</sub>	0.036	44,44,45
080319B	0.937	81.00±1.00	15-150	1173	0.03±0.01	O	0.012±0.002	0.080	44,44,62
090323	3.568	202.00 <sup>+28.00</sup> <sub>-25.00</sub>	20-10000	3722	17.80 <sup>+19.60</sup> <sub>-1.70</sub>	X	0.078 <sup>+0.032</sup> <sub>-0.003</sub>	11.4	63,63,64
090328	0.736	95.00±10.00	8-40000	100	6.40 <sup>+12.00</sup> <sub>-1.50</sub>	X	0.121 <sup>+0.085</sup> <sub>-0.011</sub>	0.729	65,65,64
090902B	1.822	374.00±3.00	50-10000	2972	6.20 <sup>+2.40</sup> <sub>-0.80</sub>	O/X	0.065 <sup>+0.009</sup> <sub>-0.003</sub>	6.27	66,67,64
090926A	2.106	145.00±4.00	8-1000	1808	9.00±2.00	O/X	0.077±0.006	5.32	68,69,64

<sup>a</sup>The energy range (keV) over which the fluence was reported.

<sup>b</sup>The isotropic gamma-ray energies ( $E_{\text{iso}}(\gamma)$ )

<sup>c</sup>The jet-break is identified in radio (R), optical (O), or X-ray (X), respectively.

<sup>d</sup>The jet opening angle ( $\theta_j$ )

<sup>e</sup>The geometrically-corrected gamma-ray energy ( $E_\gamma$ )

References. — (1) Bloom et al. 1998; (2) Piran, Jimenez, & Band 2000; (3) Frail et al. 2000; (4) Djorgovski et al. 2001; (5) Djorgovski et al. 1998; (6) Frail et al. 2003; (7) Kulkarni et al. 1999; (8) Vreeswijk et al. 2001; (9) Harrison et al. 1999; (10) Le Floc'h et al. 2002; (11) Amati et al. 2000; (12) Masetti et al. 2000; (13) Vreeswijk et al. 1999; (14) Halpern et al. 2000; (15) Castro et al. 2000a; (16) Berger et al. 2000; (17) Bloom et al. 2003; (18) Berger et al. 2001; (19) Castro et al. 2000b; (20) Price et al. 2001; (21) Harrison et al. 2001; (22) Mirabal et al. 2002; (23) in't Zand et al. 2001; (24) Galama et al. 2003; (25) Price et al. 2002; (26) Ricker et al. 2002; (27) Price et al. 2003a; (28) Holland et al. 2002; (29) Frontera et al. 2002; (30) Bloom, Frail, & Kulkarni 2003; (31) <http://space.mit.edu/HETE/Bursts/>; (32) Berger, Kulkarni, & Frail 2003; (33) Price et al. 2003b; (34) Barth et al. 2003; (35) Hurley et al. 2002; (36) Matheson et al. 2003; (37) Lamb et al. 2002; (38) Pandey et al. 2003; (39) Klose et al. 2004; (40) Andersen et al. 2003; (41) Willingale et al. 2004; (42) Jakobsson et al. 2004; (43) Stanek et al. 2005; (44) [http://heasarc.gsfc.nasa.gov/docs/swift/archive/grb\\_table/index.php](http://heasarc.gsfc.nasa.gov/docs/swift/archive/grb_table/index.php); (45) Racusin et al. 2009; (46) Butler et al. 2007; (47) Berger, Gladders, & Oemler 2005; (48) Sakamoto et al. 2005; (49) Covino et al. 2005; (50) Liang et al. 2008; (51) Cenko et al. 2006; (52) Tagliaferri et al. 2005; (53) Racusin et al. 2005; (54) Endo et al. 2005; (55) Curran et al. 2007; (56) Thöene et al. 2010; (57) Ferrero et al. 2009; (58) Krimm et al. 2007; (59) Nava et al. 2008; (60) Butler, Bloom, & Poznanski 2010; (61) Kann et al. 2007; (62) Racusin & Burrows 2008; (63) Golenetskii et al. 2009; (64) Cenko et al. 2011; (65) Rau, Connaughton, & Briggs 2009; (66) Pandey et al. 2010; (67) Bissaldi & Connaughton 2009; (68) Malesani et al. 2009; (69) Bissaldi 2009.